DOI: 10.1002/ange.201305707

Imaging Agents

Targeted Bioimaging and Photodynamic Therapy Nanoplatform Using an Aptamer-Guided G-Quadruplex DNA Carrier and Near-Infrared Light**

*Quan Yuan, Yuan Wu, Jie Wang, Danqing Lu, Zilong Zhao, Tao Liu, Xiaobing Zhang, and Weihong Tan**

Photodynamic therapy (PDT) has recently emerged as an effective, noninvasive, and economical treatment for diseases including cancers.[1] Traditional PDT suffers mainly from having an insufficient number of photons penetrating the tissue and preferentially targeting cancerous tissues with photosensitizers. Therefore, it is necessary to construct a method for controllable singlet-oxygen ($^1O_2$) generation (SOG) with high selectivity and accurate localization to provide more efficient PDT with fewer side effects.[2] Several research groups have developed novel selective PDT agents, such as peptide or protein conjugates, and photosensitizer encapsulated nanocarriers.[3] In recent years, single-stranded oligonucleotides called aptamers have emerged as a novel class of molecules which rival antibodies in both therapeutic and diagnostic applications.[4] Compared to antibodies, aptamers offer significant advantages, such as flexible design, synthetic accessibility, easy modification, chemical stability, and rapid tissue penetration.[5] Therefore, aptamers can potentially endow traditional PDT with high selectivity and accurate localization. The formation of a G-quadruplex (GQ) structure is results from a type of DNA self-assembly mode. This structure can be stabilized by a central monovalent metal cation such as potassium or sodium ions and small-molecule ligands including porphyrins.[6] Cationic porphyrins usually bind to G-quadruplexes through π–π interactions with G-quartets and through electrostatic interactions with the anionic phosphate groups on G-quadruplexes.[7] According to previous studies, some photosensitizers are porphyrin derivatives and are broadly used in PDT, such as 5,10,15,20-tetrakis-(1-methyl-4-pyridyl)-21*H*, 23*H*-porphine (TMPyP4). Therefore, the G-quadruplex DNA sequence can be a carrier for photosensitizers with porphyrin molecular structures. By taking advantage of the loading function of the G-quadruplex structure and the recognition function of aptamers, the photosensitizer can be delivered to a target cell with high affinity and selectivity.

Up to now, most photosensitizers have been activated by visible light. As a consequence, the shallow penetration depth of incident light has limited their otherwise wide applications. If the photosensitizers are linked to a visible-light generator and the generator is remotely controlled (turned on/off) by near-infrared (NIR) light, then the problem of limited depth penetration by visible light could be easily overcome. To solve the problem of limited depth penetration of current PDT techniques, we used upconversion nanoparticles (UCNPs), in particular, lanthanide-doped rare-earth nanocrystals.[8] These nanomaterials are able to emit shorter-wavelength photons under excitation by NIR light, thus making them good visible-light generators with the ability to be remotely controlled by NIR light. Furthermore, owing to the ladderlike arrangement of energy levels in lanthanide ions, UCNPs show high efficiency of photon upconversion with a distinct set of sharp emission peaks under moderate excitation densities, thereby enabling targeted bioimaging when functionalized with biomolecular recognition moieties.[9]

Herein, we report a specific aptamer-guided G-quadruplex DNA nanoplatform for targeted bioimaging and PDT, and it is capable of selective recognition and imaging of cancer cells, controllable and effective activation of the photosensitizer, and improvement of the therapeutic effect. In particular, a guanine-rich DNA segment is linked to an aptamer to form a bifunctional DNA sequence, termed a G4-aptamer. The G4-aptamer not only loads the photosensitizer but also specifically recognizes target cells. As shown in Scheme 1, the G4-aptamer is bioconjugated to a UCNP, thus placing the photosensitizer TMPyP4 at position near the UCNP for energy transfer between the UCNP and TMPyP4. Once the nanoplatform is delivered into cancer cells, the UCNPs are excited by NIR light to emit visible light to image cancer cells and, in turn, to activate TMPyP4, which, finally, generates sufficient ROS to efficiently kill cancer cells.

[*] Prof. Q. Yuan,[+] Y. Wu,[+] D. Lu, Dr. Z. Zhao, T. Liu, Prof. X. Zhang, Prof. W. Tan
Molecular Science and Biomedicine Laboratory
State Key Laboratory for Chemo/Bio-Sensing and Chemometrics
College of Chemistry and Chemical Engineering, College of Biology, and Collaborative Research Center for Chemistry and Molecular Medicine
Hunan University, Changsha 410082 (China)
E-mail: tan@chem.ufl.edu
Prof. Q. Yuan,[+] J. Wang
Key Laboratory of Analytical Chemistry for Biology and Medicine (Ministry of Education)
College of Chemistry and Molecular Sciences
Wuhan University, Wuhan 430072 (China)
[+] These authors contributed equally to this work.

[**] This work was supported by the National Key Scientific Program of China (2011CB911000), NSFC (Grant 21221003), and China National Instrumentation Program (2011YQ03012412), and the National Natural Science Foundation of China (21201133, 51272186). Q.Y. thanks Wuhan University for start-up funds and Equipment Sharing Foundation of Wuhan University.

Supporting information for this article is available on the WWW under http://dx.doi.org/10.1002/anie.201305707.

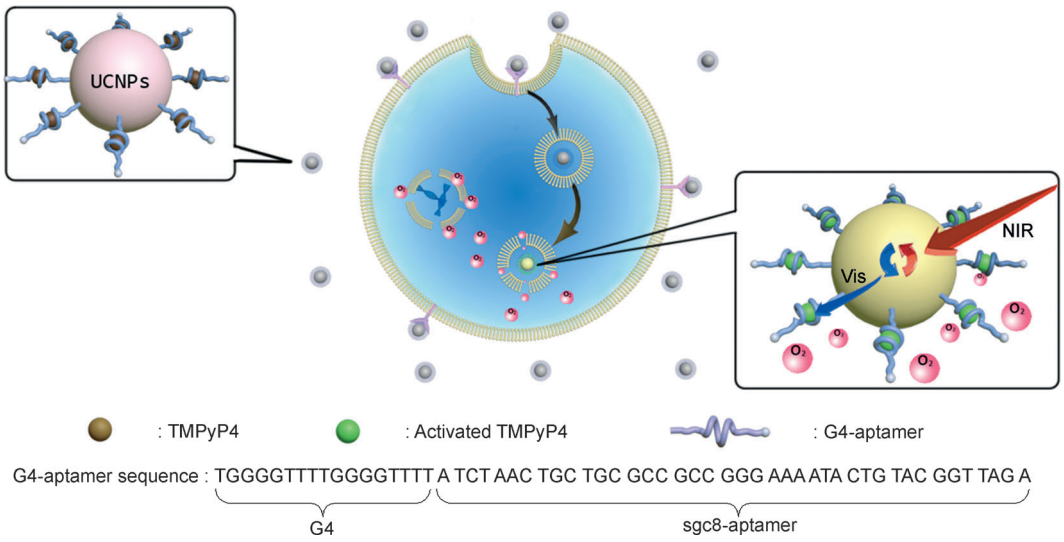

Scheme 1. Engineering of a targeted photodynamic therapy nanoplatform using an aptamer-guided G-quadruplex DNA carrier and near-infrared irradiation.

The TMPyP4 used in this study is a porphyrin derivative. Its unique symmetrical aromatic structure and cationic properties allow it to bind to and stabilize the G-quadruplex formation.[10] To achieve targeted delivery of TMPyP4, we chose a 26-mer DNA aptamer, sgc8, as the targeting aptamer. The sgc8 aptamer has been shown to have high binding affinity to the cell membrane receptor protein tyrosine kinase 7 (PTK7),[11] a protein that is over expressed on the plasma membrane of CCRF-CEM cells (CEM), a human precursor to the T-cell acute lymphoblastic leukemia (T-ALL) cell line.[12] In brief, a guanine-rich DNA segment, T-4G-4T-4G-4T, was linked with the CEM-cell-binding aptamer to construct a bifunctional G4-aptamer platform. The section nearest the 5′ end folds into a G-quadruplex structure to load TMPyP4 while the section nearest the 3′ end specifically recognizes CEM cells. Additionally, thiol modification on the 5′ terminus enables linking between the G4-aptamer and the UCNPs through the bifunctional crosslinker sulfosuccinimidyl 4-[N-maleimidomethyl] cyclohexane-1-carboxylate (Sulfo-SMCC). As shown in Scheme 2, two G4-aptamer sequences fold into GQs with the aptamers unaffected in the presence of K^+. Then, upon the addition of TMPyP4, the G4-aptamer forms a large complex with the photosensitizer. This design perfectly combines the loading function of the G-quadruplex structure with the recognition function of aptamers to compensate for the otherwise poor selectivity of photosensitizers in traditional PDT, thus in turn providing a universal strategy for the design of multifunctional platforms in biomedical applications.

After annealing in an appropriate buffer, the G-quadruplex conformation was verified by circular dichroism (CD) spectroscopy (Figure 1 a). The CD spectra and the conformations of G-quadruplexes show an empirical relationship. That is, a positive band at $\lambda = 275$ nm and negative band at $\lambda =$

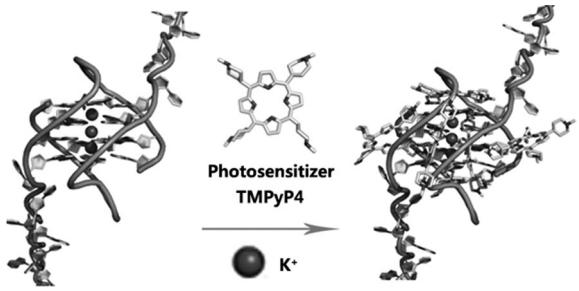

Scheme 2. Interaction between the G4-aptamer and TMPyP4.

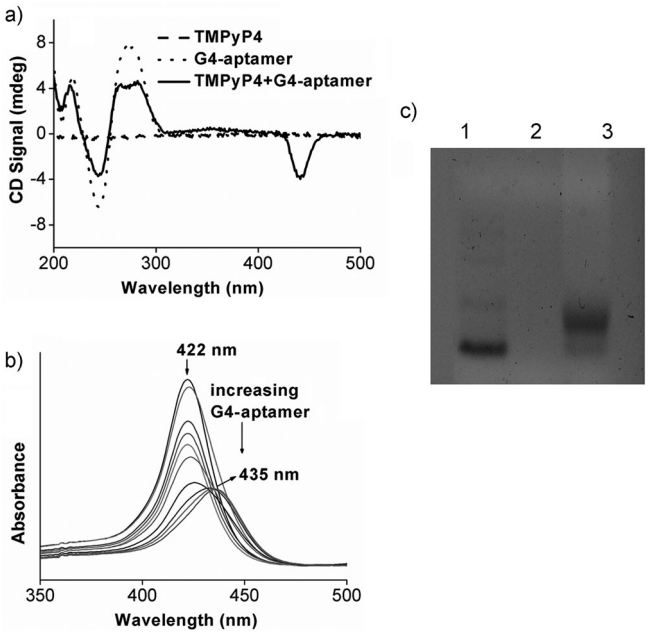

Figure 1. a) CD spectra of TMPyP4 (dashed line), the G4-aptamer (dotted line), and the TMPyP4-G4-aptamer (solid line). b) UV/Vis absorption titration spectra of TMPyP4 with the G4-aptamer. c) Agarose gel electrophoresis tests of the G4-aptamer (lane 1), TMPyP4 (lane 2), and the TMPyP4-G4-aptamer (lane 3).

250 nm represent parallel strands, whereas a positive band at $\lambda = 290$ nm and a negative band at $\lambda = 260$ nm represent antiparallel strands.[13] The negative peak at $\lambda = 250$ nm and positive peak at $\lambda = 275$ in the G4-aptamer indicated that the annealed aptamer did indeed form a parallel G-quadruplex structure. Free TMPyP4 did not show any detectable CD absorption. However, after mixing TMPyP4 with a solution of G4-aptamer, the intensities of CD bands corresponding to the G4-aptamer decreased, and a new negative peak emerged at $\lambda = 441$ nm, thus indicating the interaction between TMPyP4 and the G4-aptamer to form a TMPyP4-G4-aptamer complex.[14] The UV/Vis spectrum of TMPyP4 showed an absorption band at $\lambda = 422$ nm. However, the peak position shifted to $\lambda = 435$ nm with the addition of the G4-aptamer to the TMPyP4 solution (Figure 1b). This spectrum further demonstrated the formation of the TMPyP4-G4-aptamer complex. The agarose gel electrophoresis test (Figure 1c) showed that the G4-aptamer formed a predominant G-quadruplex structure because only one major band was observed (lane 1). The TMPyP4 showed no signals, as expected (lane 2), and lane 3 clearly indicated that the G4-aptamer formed a large structure with TMPyP4, as the electrophoretic mobility was slower than that of the G-quadruplex (lane 1). All of these results demonstrated that TMPyP4 and G4-aptamer formed a TMPyP4-G4-aptamer complex after the annealing process.

To achieve highly efficient luminescence resonance energy transfer (LRET) between the UCNP and TMPyP4 loaded on the G4-aptamer, we modified the originally synthesized hydrophobic UCNPs with polyethylenimine (PEI) to introduce amino groups, which not only enable the linking between UCNPs and G4-aptamers but also make the UCNPs hydrophilic for biological applications. As shown in Figure 2a, the thiol-modified G4-aptamer forms a covalent bond with the Sulfo-SMCC linked to amino group on the surface of a UCNP to construct a UCNP-G4-aptamer. FT-IR (see Figure S2 in the Supporting Information) and Zeta potential (see Figure S3 in the Supporting Information) measurements have been performed to verify each modification step. Then TMPyP4 is effectively loaded into the G-quadruplex structure, thus creating the proper distance for energy transfer between the two components to achieve effective activation of TMPyP4 by the UCNPs.

$NaLuF_4$ nanocrystals doped with 12% Gd, 50% Yb, and 2% Er ($NaLuF_4$:12% Gd,50% Yb,2% Er) were synthesized following a previously reported protocol.[15] Our synthesized $NaLuF_4$-based UCNPs showed uniform sizes with an average diameter of approximately 15 nm, as shown in Figure 2b. Typical XRD patterns of the as-prepared UCNPs are presented in Figure 2c. The diffraction peaks of the NPs are well-defined, and the peak positions and intensities agree well with the calculated values for hexagonal NaLuF4, thus indicating that the as-prepared NPs are a highly crystalline pure hexagonal phase. The upconversion luminescence spectrum of the UCNP-G4-aptmer displayed characteristic blue, green, and red emission bands corresponding to the transitions from the emitting energy levels of the Er ions as illustrated (Figure 2d). The blue emission from UCNPs is well matched with the absorption peak of TMPyP4, and the energy

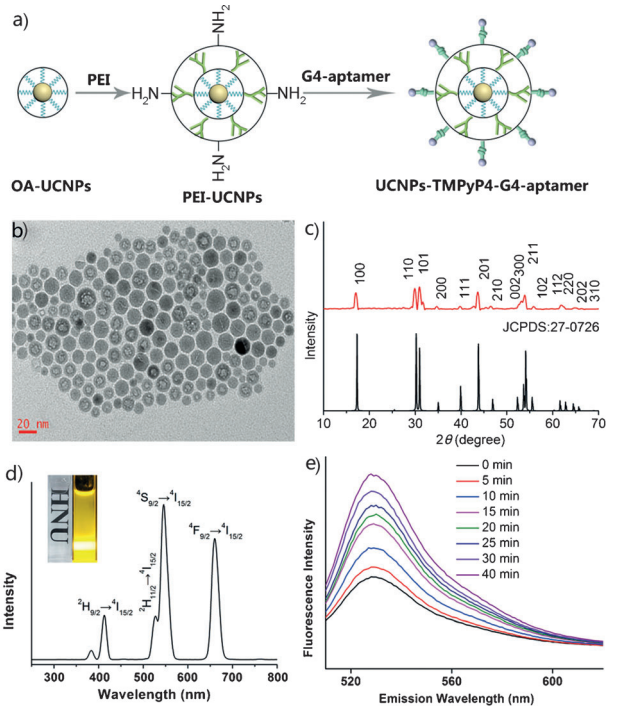

Figure 2. a) Construction of the nanoplatform. b) TEM image of as-synthesized $NaLuF_4$:12%Gd,50%Yb,2%Er. c) X-ray diffraction (XRD) pattern of $NaLuF_4$:12%Gd,50%Yb,2%Er (top) compared to the standard spectrum (bottom). d) Room-temperature upconversion luminescence spectra of the UCNP-G4-aptamer in water. Insert: corresponding luminescence photographs. e) Determination of singlet oxygen through the strong fluorescence of singlet oxygen sensor green (SOSG) upon oxidation by singlet oxygen.

transfer from UCNPs to TMPyP4 enables indirect activation of the photosensitizer by NIR light. The UCNP-G4-aptamer possesses excellent water solubility, as shown in the insert of Figure 2d. Upon continuous-wave excitation at $\lambda = 980$ nm, the luminescence of the particles in water appears predominantly yellow in color from a combination of green and red emissions from the Er^{3+} ion. Generation of cytotoxic singlet oxygen is critical in photodynamic cancer cell therapy, as it directly leads to target cell apoptosis. The production of a SOG by the UCNP-TMPyP4-G4-aptamer using laser irradiation at $\lambda = 980$ nm was quantified by measuring the fluorescence of singlet oxygen sensor green (SOSG), which can be specifically oxidized by singlet oxygen to produce enhanced fluorescence upon oxidation.[16] As shown in Figure 2e, SOSG fluorescence increased 2.5-fold over a span of 40 minutes, and illustrates that singlet oxygen can be efficiently generated from the cooperation of the UCNP and TMPyP4 through a LRET process.

In this design, sgc8, which binds to the cancer cell membrane protein PTK7 with high affinity and selectivity ($K_d = (0.8 \pm 0.09)$ nM), was used to equip the UCNPs with targeted bioimaging capability. CCRF-CEM with high PTK7 expression was used as the target cancer cell and Ramos (acute lymphoblastic leukemia B-cells) without PTK7 was used as a negative control cell. As shown in Figure 3a, CEM cells incubated with the UCNP-G4-aptamer showed strong

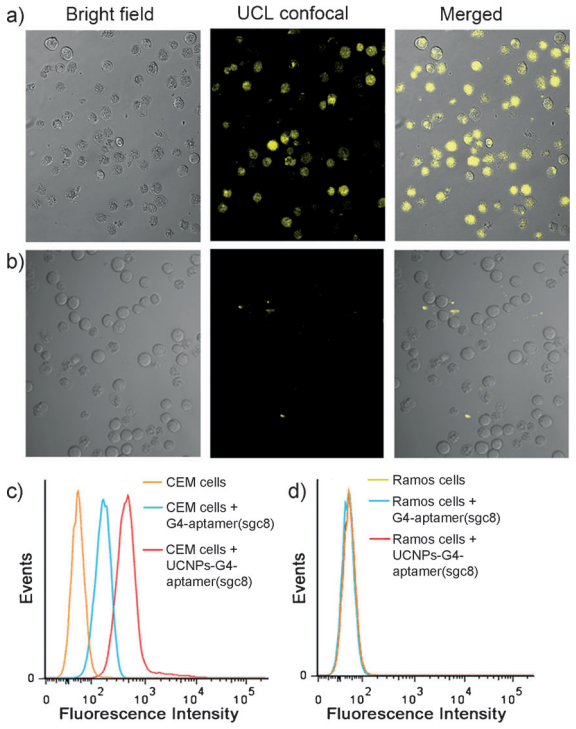

Figure 3. Confocal microscopy images of a) CEM cells (target cells) and b) Ramos cells (control cells) treated with the UCNP-G4-aptamer. Flow cytometry histograms to monitor the binding of the G4-aptamer and UCNP-G4-aptamer with c) CEM cells and d) Ramos cells, respectively.

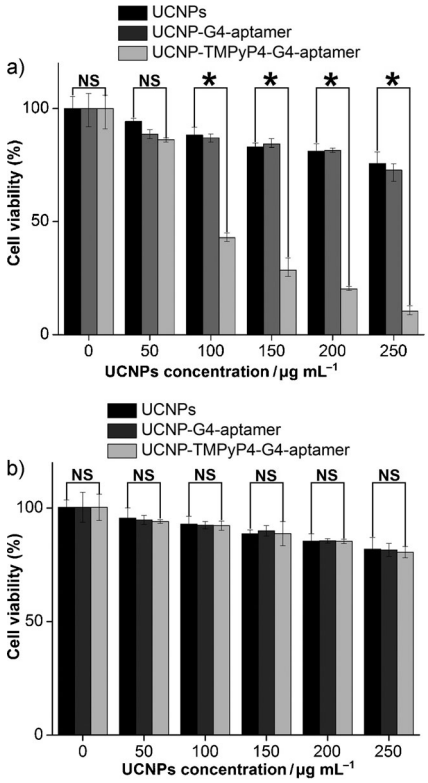

Figure 4. Cytotoxicity assay of a) CEM cells (target cells) and b) Ramos cells (control cells) treated with UCNPs, UCNP-G4-aptamer, and UCNP-TMPyP4-G4-aptamer. P values were calculated by the t-test. $P > 0.05$ and * for $P < 0.05$, $n = 3$. NS = not significant.

fluorescence within the cells, whereas the UCNP-G4-aptamer exhibited much less binding and internalization ability when incubated with Ramos cells (Figure 3b). These data clearly indicated that sgc8 showed great selectivity for CEM cells, thus leading to the targeted bioimaging ability of the UCNP-G4-aptamer. The targeting specificity of sgc8 toward CEM cells was also confirmed by flow cytometry, as shown in Figures 3c,d. The aptamer was labeled with 6-carboxyfluorescein (FAM). In this case, sgc8 was used as a positive control. Compared to sgc8, the UCNP-G4-aptamer showed a stronger binding affinity to CCRF-CEM cells at 37 °C. However, both sgc8 and the UCNP-G4-aptamer exhibited weak affinity to the control Ramos cells, as evidenced by only small fluorescence peak shifts (Figure 3d). These results demonstrated that our UCNP-G4-aptamer could bind to and be internalized by CEM cells with high selectivity but showed little affinity to nontarget cells, thus indicating, in turn, that the aptamer-guided G-quadruplex DNA nanoplatform we developed could be used as a targeted luminescent probe for living cells in bioimaging.

The NIR light triggered PDT of cancer cells was investigated by measuring cell viability using the MTS assay. Both cell lines were treated with either UCNPs or the UCNP-G4-aptamer under laser irradiation and showed negligible cell death even at concentrations up to 250 $\mu g\,mL^{-1}$ (Figures 4a,b), thus indicating excellent biocompatibility of the nanocarriers. However, significantly reduced cell viabilities were observed for CEM cells (Figure 4a) incubated with the UCNP-TMPyP4-G4-aptamer of more than 100 $\mu g\,mL^{-1}$ after exposure to the $\lambda = 980$ nm laser (10 min, 1 min intervals, 0.5 $W\,cm^{-2}$). The cell viabilities were $(42.9 \pm 1.4)\,\%$ (mean $\pm$SD) for CEM cells treated with the UCNP-TMPyP4-G4-aptamer at a concentration of 100 $\mu g\,mL^{-1}$, while the cell viabilities were $(88.2 \pm 2.1)\,\%$ and $(87.0 \pm 3.5)\,\%$ after treatment with UCNPs and the UCNP-G4-aptamer, respectively, at the same concentrations. These results showed that high phototoxicity was generated by the UCNP-TMPyP4-G4-aptamer compared to UCNPs with $P < 0.05$. By increasing the concentration of the UCNP-TMPyP4-G4-aptamer, the cell viability reduced to $(28.6 \pm 3.1)\,\%$ (150 $\mu g\,mL^{-1}$), $(20.3 \pm 1.3)\,\%$ (200 $\mu g\,mL^{-1}$), and $(10.4 \pm 2.7)\,\%$ (250 $\mu g\,mL^{-1}$), and these three groups correspondingly showed that the UCNP-TMPyP4-G4-aptamer could generate increasingly greater phototoxicity to CEM cells with $P < 0.05$.

In contrast to the dramatic enhancement in phototoxicity effects for the UCNP-TMPyP4-G4-aptamer on CEM cells, a much less pronounced phototoxicity to Ramos cells was observed for the UCNP-TMPyP4-G4-aptamer, with cellular viability of $(91.9 \pm 2.2)\,\%$, $(88.4 \pm 3.8)\,\%$, $(85.0 \pm 2.0)\,\%$, and $(80.3 \pm 2.8)\,\%$ for four samples having a concentration of 100, 150, 200, and 250 $\mu g\,mL^{-1}$ ($P > 0.05$), respectively. These data suggest that this NIR light triggered nanoplatform provides the conditions required for improved and selective cytotoxicity to target cancer cells for the following reasons: 1) Aptamer functionalization enables specific binding to CEM cells, followed by selective internalization of the

nanoplatform. 2) TMPyP4 is suitably distant from UCNP in the G-quadruplex DNA structure, thus allowing highly efficient LRET to occur. 3) Compared to UV or visible light, NIR light penetrates more deeply into cells or tissues, thus causing less damage to normal cells.

In summary, we combined the beneficial features of a DNA aptamer with 1) the intercalation of photosensitizer TMPyP4 within the G-quadruplex DNA structure and 2) NIR light triggered upconversion nanomaterials to develop a smart cancer-specific imaging and photodynamic therapy system. Utilizing sgc8 as a model for targeting, selective cancer cell photodynamic therapy is realized using $\lambda = 980$ nm irradiation by resonance energy transfer from hexagonal-phase NaLuF4:12 % Gd,50 % Yb,2 % Er UCNPs to photosensitizer molecules. The unique upconversion luminescence emission from UCNPs also provides a way for targeted cell labeling and tracking, which will possibly be useful for future imaging-guided therapy studies. We anticipate that the UCNP-G4-aptamer-drug platform may be utilized to develop novel effective cancer chemotherapy methodologies.

Received: July 2, 2013
Revised: August 5, 2013
Published online: November 26, 2013

Keywords: aptamer · G-quadruplexes · imaging agents · nanoparticles · singlet oxygen

[1] J. P. Celli, B. Q. Spring, I. Rizvi, C. L. Evans, K. S. Samkoe, S. Verma, B. W. Pogue, T. Hasan, *Chem. Rev.* **2010**, *110*, 2795 – 2838.

[2] Z. Zhu, Z. W. Tang, J. A. Phillips, R. H. Yang, H. Wang, W. H. Tan, *J. Am. Chem. Soc.* **2008**, *130*, 10856 – 10857.

[3] a) A. R. Oseroff, D. Ohuoha, T. Hasan, J. C. Bommer, M. L. Yarmush, *Proc. Natl. Acad. Sci. USA* **1986**, *83*, 8744 – 8748; b) S.-I. Ogura, K. Yazaki, K. Yamaguchi, T. Kamachi, I. Okura, *J. Controlled Release* **2005**, *103*, 1 – 6; c) Y. Choi, R. Weissleder, C. H. Tung, *Cancer Res.* **2006**, *66*, 7225 – 7229.

[4] a) Y. Huang, G. D. Shang, H. Liu, J. A. Phillips, X. Zhang, Y. Chen, W. Tan, *ChemBioChem* **2009**, *10*, 862 – 868; b) L.-L. Li, Q. Yin, J. Cheng, Y. Lu, *Adv. Healthcare Mater.* **2012**, *1*, 567 – 572; c) Y. Du, B. Li, E. Wang, *Acc. Chem. Res.* **2013**, *46*, 203 – 213.

[5] W. H. Tan, M. J. Donovan, J. H. Jiang, *Chem. Rev.* **2013**, *113*, 2842 – 2862.

[6] Y. A. Shieh, S. J. Yang, M. F. Wei, M. J. Shieh, *ACS Nano* **2010**, *4*, 1433 – 1442.

[7] a) P. Zhang, W. Steelant, M. Kumar, M. Scholfield, *J. Am. Chem. Soc.* **2007**, *129*, 4526 – 4527; b) R. Weissleder, V. Ntziachristos, *Nat. Med.* **2003**, *9*, 123 – 128; P. Zhang, S. Rogelj, K. Nguyen, D. Wheeler, *J. Am. Chem. Soc.* **2006**, *128*, 12410.

[8] a) L. Li, R. Zhang, L. Yin, K. Zheng, W. Qin, P. R. Selvin, Y. Lu, *Angew. Chem.* **2012**, *124*, 6225 – 6229; *Angew. Chem. Int. Ed.* **2012**, *51*, 6121 – 6125; b) Q. Ju, D. Tu, Y. Liu, R. Li, H. Zhu, J. Chen, Z. Chen, M. Huang, X. Chen, *J. Am. Chem. Soc.* **2012**, *134*, 1323 – 1330; c) F. Wang, Y. Han, C. S. Lim, Y. H. Lu, J. Wang, J. Xu, H. Y. Chen, C. Zhang, M. Hong, X. Liu, *Nature* **2010**, *463*, 1061 – 1065; d) H. Mai, Y. Zhang, R. Si, Z. Yan, L. Sun, L. You, C. Yan, *J. Am. Chem. Soc.* **2006**, *128*, 6426 – 6436; e) L. Wang, R. Yan, Z. Huo, L. Wang, J. Zeng, J. Bao, X. Wang, Q. Peng, Y. Li, *Angew. Chem.* **2005**, *117*, 6208 – 6211; *Angew. Chem. Int. Ed.* **2005**, *44*, 6054 – 6057; f) L. Cheng, K. Yang, Y. Li, J. Chen, C. Wang, M. Shao, S. Lee, Z. Liu, *Angew. Chem.* **2011**, *123*, 7523 – 7528; *Angew. Chem. Int. Ed.* **2011**, *50*, 7385 – 7390.

[9] a) M. Wang, C. C. Mi, W. X. Wang, C. H. Liu, Y. F. Wu, Z. R. Xu, C. B. Mao, S. K. Xu, *ACS Nano* **2009**, *3*, 1580 – 1586; b) T. Zako, H. Nagata, N. Terada, A. Utsumi, M. Sakono, M. Yohda, H. Ueda, K. Soga, M. Maeda, *Biochem. Biophys. Res. Commun.* **2009**, *381*, 54 – 58.

[10] a) A. De Cian, L. Lacroix, C. Douarre, N. Temime-Smaali, C. Trentesaux, J. F. Riou, J. L. Mergny, *Biochimie* **2008**, *90*, 131 – 155; b) C. Granotier, G. Pennarun, L. Riou, F. Hoffschir, L. R. Gauthier, A. De Cian, D. Gomez, E. Mandine, J. F. Riou, J. L. Mergny, P. Mailliet, B. Dutrillaux, F. D. Boussin, *Nucleic Acids Res.* **2005**, *33*, 4182 – 4190.

[11] a) K. Mossie, B. Jallal, F. Alves, I. Sures, G. D. Plowman, A. Ullrich, *Oncogene* **1995**, *11*, 2179 – 2184; b) X. Lu, A. G. Borchers, C. Jolicoeur, H. Rayburn, J. C. Baker, M. Tessier-Lavigne, *Nature* **2004**, *430*, 93 – 98.

[12] D. Shangguan, Y. Li, Z. Tang, Z. C. Cao, H. W. Chen, P. Mallikaratchy, K. Sefah, C. J. Yang, W. Tan, *Proc. Natl. Acad. Sci. USA* **2006**, *103*, 11838 – 11843.

[13] a) S. Burge, G. N. Parkinnson, P. Hazel, A. K. Todd, S. Neidle, *Nucleic Acids Res.* **2006**, *34*, 5402 – 5415; b) X. H. Cheng, X. J. Liu, T. Bing, R. Zhao, S. X. Xiong, D. H. Shangguan, *Biopolymers* **2009**, *91*, 874 – 883; c) C. C. Hardin, A. G. Perry, K. White, *Biopolymers* **2001**, *56*, 147 – 194; d) V. Dapic, V. Abdomerovic, R. Marrington, J. Peberdy, A. Rodger, J. O. Trent, P. J. Bates, *Nucleic Acids Res.* **2003**, *31*, 2097 – 2107.

[14] a) H. J. Zhang, X. Xiao, P. Wang, S. P. Pang, F. Qu, X. C. Ai, J. P. Zhang, *Spectrochim. Acta Part A* **2009**, *74*, 243 – 247; b) L. Martino, B. Pagano, I. Fotticchia, S. Neidle, C. Giancola, *J. Phys. Chem. B* **2009**, *113*, 14779 – 14786; c) Y. Nitta, R. Kuroda, *Biopolymers* **2006**, *81*, 376 – 391.

[15] Q. Liu, S. Yun, T. S. Yang, W. Feng, C. G. Li, F. Y. Li, *J. Am. Chem. Soc.* **2011**, *133*, 17122 – 17125.

[16] a) Z. Tang, Z. Zhu, P. Mallikaratchy, R. Yang, K. Sefah, W. Tan, *Chem. Asian J.* **2010**, *5*, 783 – 786; b) B. M. Barth, I. E. Altinoglu, S. S. Shanmugavelandy, J. M. Kaiser, D. Crespo-Gonzalez, N. A. DiVittore, C. McGovern, T. M. Goff, N. R. Keasey, J. H. Adair, et al., *ACS Nano* **2011**, *5*, 5325 – 5337.

